Geophysical Journal International

Geophys. J. Int. (2011) **186,** 699–705 doi: 10.1111/j.1365-246X.2011.05051.x

Low cost volcano deformation monitoring: optical strain measurement and application to Mount St. Helens data

Thomas R. Walter

Dept. 2: Physics of the Earth, Helmholtz Centre Potsdam – GFZ German Research Centre for Geosciences, Telegrafenberg, 14473 *Potsdam, Germany.*
E-mail: twalter@gfz-potsdam.de

Accepted 2011 April 21. Received 2011 March 23; in original form 2010 December 1

SUMMARY

This paper describes an innovative method of volcano deformation measurements, applied to camera images taken from the 2004–2008 eruption period at Mount St. Helens. Dome growth was thought to be characterized by sustained, near-linear rates of a solid dacite plug. Through spatial digital image correlation (DIC) analysis of the camera images, new evidences arise that the deformation and strain rate of the spine was more complex. DIC yielded cumulative and incremental displacements, strain and shear planes at decimetre resolution. It was found that dome extrusion rates are highly non-linear, decelerating prior to partial collapse, followed by a pronounced dome extrusion increase and direction change. Associated processes have been identified through DIC, such as shallow landslides and reworking of talus apron material. The work highlights the strengths of camera strain monitoring, and illustrates that dome growth and collapse is a very dynamic process complexly interplaying with the surrounding.

Keywords: Image processing; Eruption mechanisms and flow emplacement; Remote sensing of volcanoes; Volcano monitoring.

1 INTRODUCTION

Volcano monitoring means the observation of the state of a (volcanic) system, requiring both temporal and spatial information. Advances in geodetic volcano monitoring technologies focused mainly on satellite based technologies, such as InSAR (Dzurisin 2007). The main benefit of these techniques in comparison to direct field surveying methods is that through remotely sensed data streams the state of a volcano's activity, whether erupting or not, might be observed at spatial resolution from safe distance even in high risk areas and regions that are difficult to assess. In addition, the visual observation and monitoring is used at most volcano observatories, however, quantitative optical monitoring has remained sparse. The strength of optical image correlation has been applied mainly to satellite images observing landslides (Delacourt *et al.* 2004), permafrost deformation and glacier flows (Scambos *et al.* 1992; Kaab 2002; Berthier *et al.* 2005), and earthquakes (Van Puymbroeck *et al.* 2000). Using a fixed camera inflation associated with an volcano eruption could be analysed (Johnson *et al.* 2008). As this study shows, the presence of cameras, possibly web-cams, installed at potentially dangerous volcanoes significantly contributes to spatial deformation monitoring. Illustrated for images available for the Mount St. Helens 2006 spine extrusion, this paper shows the strengths and added value of modern digital image correlation technologies, applicable to almost any digital and optical dataset at volcanoes elsewhere.

Extrusion of dacitic magma through the pre-existing glaciated 2-km-wide amphitheatre of Mount St. Helens commenced in 2004. During the eruption period of Mt. St. Helens from 2004 to 2008, several spines of highly viscous lava have been extruded at a location just south of the 1980–1986 dome (Fig. 1). The new eruption period has been distinguished into five main phases (Vallance *et al.* 2008). According to earlier workers the magma was 'solid', being poor in gasses (Gerlach *et al.* 2008) and rich in crystals (Pallister *et al.* 2008). The morphometry and locations of individual spine extrusion was highly dynamic though, including vertical and lateral (recumbent) spine growth, whaleback formation, incorporation of older rocks (compound spines), comprehensively summarized in Vallance *et al.* (2008). In the 2004–2008 extrusion sequence at least seven distinguished spines have been identified, which have been closely and successfully monitored using geophysical, geochemical and geological technologies (Sherrod *et al.* 2008).

The aim of this work is to focus on the analysis of optical data recorded by fixed camera installations (Major *et al.* 2008; Poland *et al.* 2008). From 2004 onwards an extensive implementation of cameras allowed to visually investigate spine growth and dynamics of the Mount St. Helens crater. Besides providing important information on the weather condition, cameras showed to be of high importance for visualization of the state of volcanic activity, and provide a visual data stream adding to other monitoring methods (Poland *et al.* 2008). The Mount St. Helens camera data so far have not been analysed in their full spatial dimension, where the amplitude pattern of hundreds of thousands of identifiable pixels can be evaluated to explore the deformation field.

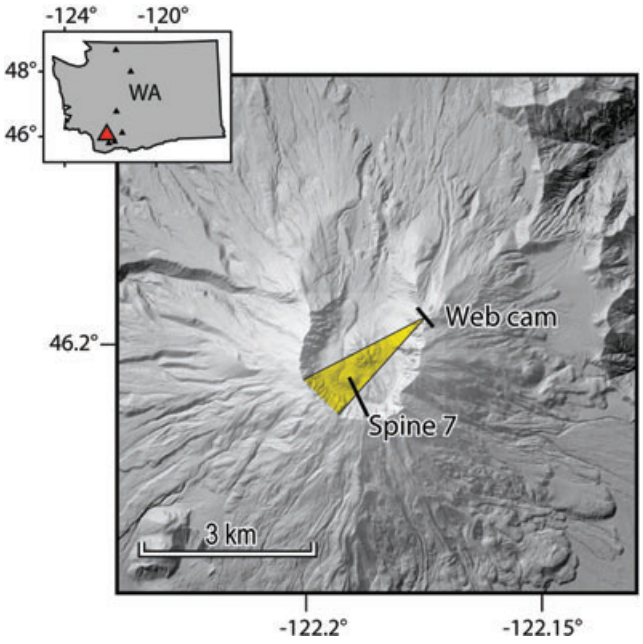

Figure 1. Inset shows location of Mount St. Helens within the state of Washington, USA (upper left-hand side). Digital elevation map shows Mount St. Helens, and location of the USGS camera ('Brutus') used for the purpose of this study. The camera was at distance of 1.2 km from the dome and focused on the so-called spine 7, which is the 7th of consecutively identified spines.

2. METHOD

DIC allows displacement detection with a resolution that is about 2 orders of magnitudes better than detectable by eye (Hauser & Walz 2004) by considering mathematical cross-correlation of a digital photography dataset that consists of a 2-D matrix of intensity values $I(U)$. The method used is standard in computer vision (Pan *et al.* 2009), thus only basic principles are summarized in here. Signal intensities are recorded in at least two images from same optical parameters, and located in an orthogonal system in the image space, defined for a given pixel at a coordinate $U = (x, y)$. By computing the perturbation of an image as a shifted copy of the reference image, for a data set of $n > 2$ images the image intensity function $I(x, y, t)$ is given by the following equation (Horn & Schunck 1981):

$$I(x, y, t) = I(x + u, y + v, t + \delta t), \tag{1}$$

where (u, v) is the displacement at time δt. Following (Adrian 1991) we adaptively divide the photographs into a grid of sub-regions, each with a given dimension $N \times N$ (here, from 32×32 decreasing to 16×16 pixels with 50 per cent overlap) hosts information obtained from at least two acquisitions, the image master I_M and the image slave I_S (Fig. 2b). The squared Euclidean distance between the two sub-regions is given for $n = [N/2]$ by

$$d^2(u, v) = \sum_{x=-n}^{n} \sum_{y=-n}^{n} [I_M(x, y) - I_S(x + u, y + v)]^2. \tag{2}$$

This operation aims pairing each pixel with a corresponding pixel. Assuming that the given image intensity $\sum I_S^2(x + u, y + v)$ is almost constant, the cross-correlation term may be reformulated and allows to quantify the similarity between the subregions:

$$c(u, v) = \sum_{x=-n}^{n} \sum_{y=-n}^{n} I_M(x, y)\, I_S(x + u, y + v). \tag{3}$$

This simplified approach is widely used, though has limitations (Clocksin *et al.* 2002), arising mainly from variations of the image intensity $\sum I_S^2(x + u, y + v)$ in the space domain, the dependency of $c(u, v)$ on the feature dimension, and dependency of eq. (3) caused by changes in illumination direction, for example, in temporally sun exposed landscapes. These limitations can be overcome by normalizing $c(u, v)$ as summarized in (Clocksin *et al*. 2002), where in a simple form:

$$c'(u, v) = \frac{\sum_x \sum_y I_M(x, y)\, I_S(x + u, y + v)}{\sqrt{\sum_y \sum_y I_M^2(x, y) \sum_y \sum_y I_S^2(x + u, y + v)}}. \tag{4}$$

In the case of the Mount St. Helens dome photos, one observation was that feature rotation and transformation occurred (e.g. due to structural disintegration during collapse). The problem of such non-rigid distortions has been solved by relating the pixel coordinates in the master image with coordinates in the slave image by use of a parametric form (Schreier *et al*. 2000)

$$\zeta(x, y, \boldsymbol{\theta}) = \theta_1 + \theta_3 x + \theta_4 y \tag{5}$$

$$\eta(x, y, \boldsymbol{\theta}) = \theta_2 + \theta_5 x + \theta_6 y, \tag{6}$$

where displacement components (u, v) are described by parameters (θ_1, θ_2) are so that eq. (4) may be reformulated (Schreier *et al.* 2000) to

$$c'(u, v) = \frac{\sum_x \sum_y I_M(x, y)\, I_S[\xi(x, y, \boldsymbol{\theta}), \eta(x, y, \boldsymbol{\theta})]}{\sqrt{\sum_x \sum_y I_M^2[\xi(x, y, \boldsymbol{\theta}), \eta(x, y, \boldsymbol{\theta})] \sum_x \sum_y I_S^2[\xi(x, y, \boldsymbol{\theta}), \eta(x, y, \boldsymbol{\theta})]}}. \tag{7}$$

To apply eq. (7) to strain mapping, we are maximizing the posterior probability of displacement (Chivers & Clocksin 2000). Considering two successive images of the Mount St. Helens photo sequence separated by time, one obtains a pixel offset estimation by optimizing the cross-correlation function equation.

The 24 images (Fig. 2a) are first transformed into the frequency domain using a fast Fourier transform, followed by the cross-correlation function equation in the frequency domain (Quinta da Fonseca *et al.* 2005). Through bicubic interpolation of the region in the vicinity of an integer peak (e.g. a bright pixel), one obtains the displacement vector at subpixel resolution, specifically yielding a resolution of 0.05 pixels or 0.07 m in this study. By postprocessing pixel offset estimations the total and relative displacements at any pixel and the relative position and dislocation with respect to neighbouring observations is obtained in time. The latter may allow grouping pixels and estimation of strain components.

3 RESULTS

The camera used for the purpose of this study and demonstration (Olympus C-3030Z) was installed in 2005 August, and is located at 2479 m altitude on the northeast crater rim at N46.2061° W122.1794° (Major *et al.* 2009). The distance is about 1225 m to the east–northeast of the observed centre of the spine, with a near horizontal field of view of 21° with 1280×960 resolution (Major *et al.* 2009). A down-sampled data set was used herein for reducing processing time, with 640×480 pixels, yielding a time series at about 300 000 pixels and a mean resolution of features of ~1.4

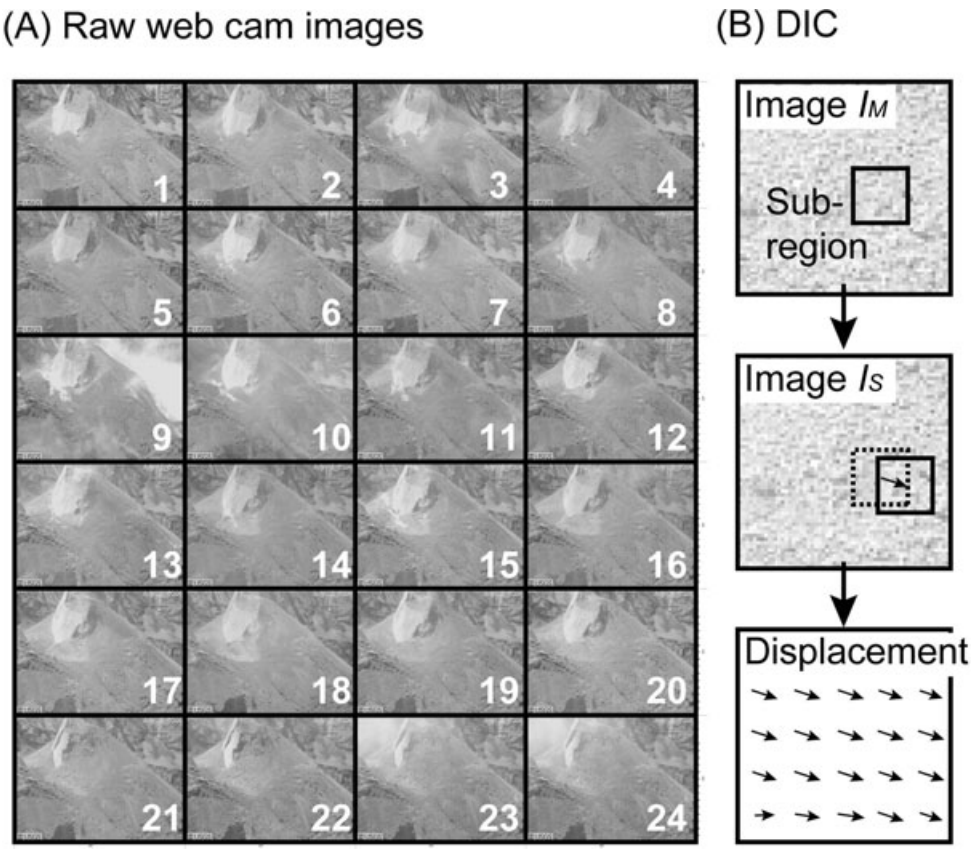

Figure 2. (a) Camera images used for the purpose of this study (Major *et al.* 2009). The selected images are temporally separated by one day. (b) Digital image correlation considers the mathematical comparison and detection of a shifted copy of subwindows in one or several following images.

m at the spine. Thus applying above methodology of digital image cross correlation allows displacement detections on the centimetre scale.

The field of view included the western part of the dome complex and the west arm of the glacier. The sequence of daily images starts on 2006 July 3 and ends on 2006 July 28, having 24 images showing the growth of the spine. Visual inspection of the camera images and a time-lapse video provided by USGS (Major *et al.* 2009) shows that the spine is growing cumulatively (Fig. 3b). Using DIC, below two postprocessing results are presented, that is, the cumulative deformation and the incremental deformation result.

(i) Cumulative deformation (Fig. 3): The cumulative displacement is computed to reduce the signal-to-noise ratio and explore the continued deformation pattern at the Mount St. Helens spine. Displacement vectors clearly show the spine and increase in length with time (Fig. 3a). Not only the vector length of the spine increase, but also a relatively shallow slump on the right-hand side of the field of view is detected. In addition, minor displacements are observed at the foot of the spine, where talus apron is reworked into the contact area of the spine. Small but continued glacial movement is observed on the right (western) side behind the spine. Cumulative invariants (scalar quantities) of the strain tensor are shown by volumetric (Fig. 3b) and maximum-shear strains (Fig. 3c). Most pronounced, the contact line between the spine and its talus apron is shown as an extensional strain region. Internally the spine shows no identifiable strain, neither compression nor extension. At the upper most part of the spine, contraction is suggested, which probably is a consequence of the image reference system, here being a stable background versus an upwardly moving spine (i.e. the vertical cliffs of Mount St. Helens crater are assumed to be stable). Shear strain (Fig. 3c) shows left lateral shear on the left-hand side, and right lateral on the right-hand side of the spines talus contact. Again no internal shear is observed within the spine, confirming its extrusion as a coherent and solid block as suggested by earlier workers. The slumping region to the right of the field of view, bordering the upper half of the spine, is clearly outlined by a listric right lateral shear plane at the base. Thus the representation of the shear strain was found useful for landslide assessment, too.

(ii) Incremental displacement (Fig. 4): The displacement between two successive images was calculated. The vector field shows the fast and uniform vertical movement of the spine in the first images, with a near constant rate until July 9. Expressed in this view is that, although the spine extrusion is near constant, slumping of the flank is highly discontinuous in time, being slow on July 4, increasing till July 8, decreasing again thereafter. From July 10 onwards, the spine movement is decelerated until July 24. On July 25 a part of the spine collapses causing a loss in coherence, thus a high noise level in the data. On July 26 the vectors are large again affecting the entire spine again, though directed not vertically but inclined at a mean 71° to the upper right-hand corner of the field of view (i.e. to the west). Associated with this sudden change, also the slump feature accelerates and changes direction from slope parallel to sub horizontal motion. Therefore the incremental displacement study, provides additional hints to the non-linear extrusion rate and slope instability of the dacitic spine of Mount St. Helens.

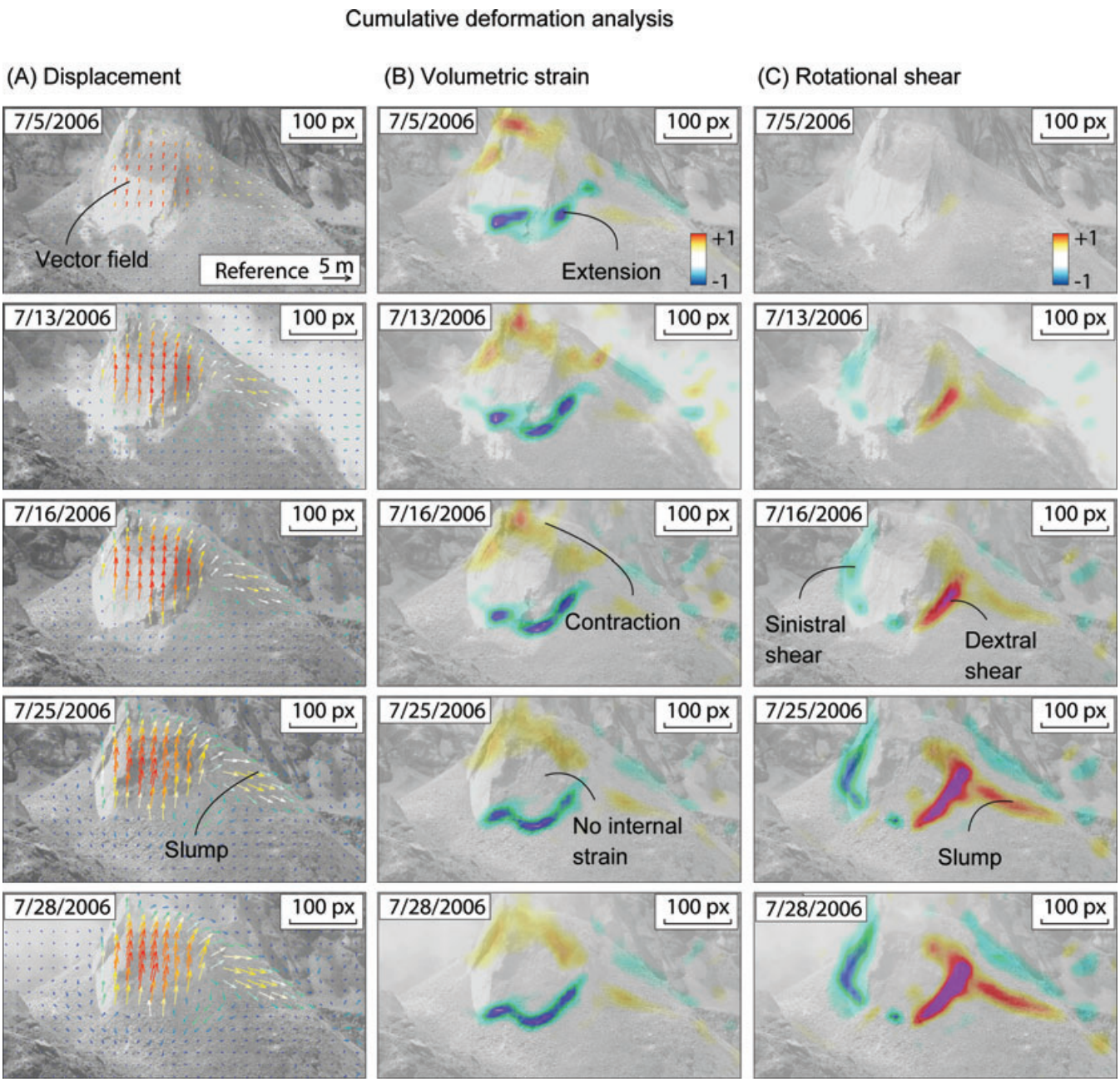

Figure 3. Cumulative deformation analysis during the 24-d observation period for selected days (from top row to bottom: July 5, July 13, July 16, July 25, July 28). (a) Displacement vectors show an increasing cumulative vector length at the dome, at a slump and at the glacier in the background. Vector length is colour coded to the deformation amplitude, red being maximal, given is the mean vector of a sub region. (b) Volumetric strain computation show no detectable internal deformation. High strain areas delimit the extruding spine. Blue is extension, red is contraction. (c) Rotational shear again delimits the extruding spine, but very clearly shows also the slump detachment plane. The upper edge of the slump also displays the relative subwindow rotation of the slump against the stable background, which is an artefact of the processing routine. One pixel translates to 1.4 m, the 100 px scale is shown in all images, the reference displacement vector is shown in the first image.

4 DISCUSSION

Visual observations of volcano unrest and eruption is one of the most important means of validating alert levels and geophysical and geochemical monitoring data. Camera and web-cam time lapse data records are low cost and low maintenance (Poland *et al.* 2008). As this work suggest, camera data may provide a very useful or even unique information source of displacement and strain rates in both the spatial and temporal dimension, contributing to a better understanding of the physical behaviour and process couplings at active volcanoes.

Limitations of the results may be based on the reduction of a 3-D displacement field to a 2-D optical array. The use of a single camera provides only a 2-D displacement field, the system is blind to the line-of-sight displacement. The results are to be considered mainly qualitative, as pixels moving towards or away from

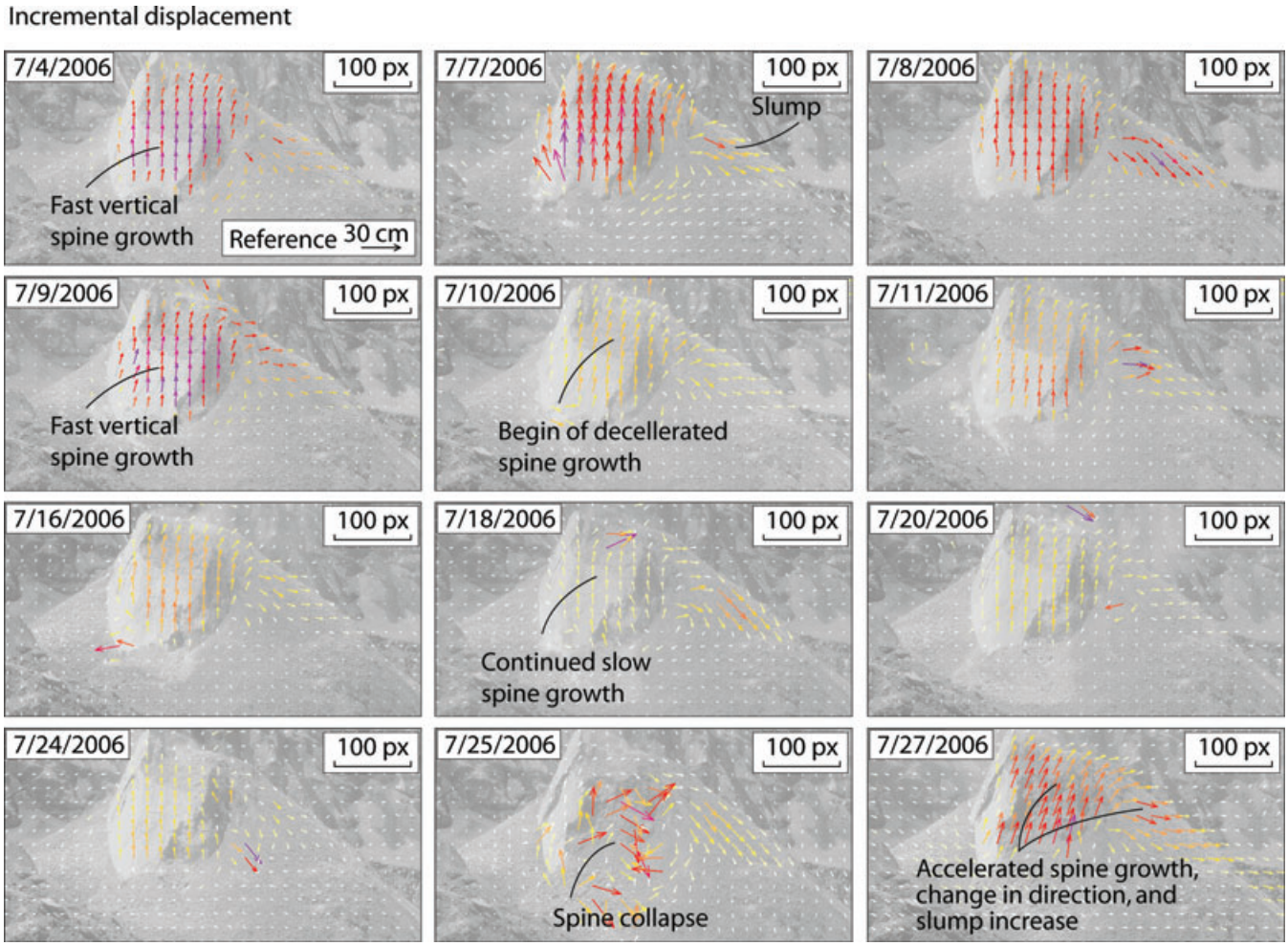

Figure 4. Incremental displacement obtained by two successive image correlation, shown here for a selection of 16 of 24 images (from top left- to bottom right-hand side: July 4, 7, 8, 9, 10, 11, 16, 18, 20, 24, 25, 27). Analysis shows that at early stages the spine is growing fast (red vectors), associated with a shallow slump on the right-hand side. Then spine growth as well as shallow slump decelerates. At later stages a collapse of the spine occurs, immediately followed by an increase in spine growth rates as well as slumping activity. This suggest a direct coupling between spine growth rates and gravity forces loading the conduit.

the camera are not detected. Ideally, cross validation with independent methods such as GPS are to be considered, though not available for the studied case example. Therefore, although the results shown in this work concerning rate changes appear generally robust, absolute displacement amplitudes and directions given need to be considered with care. Future work will need to combine at least two cameras from different position with known baseline, so that through stereoscopy a 3-D displacement monitoring can be achieved. The Mount St. Helens dome growth is now monitored with cameras from different directions, the images radio-telemetered to the Cascades volcano observatory in real time (Dzurisin *et al*. 2008; Major *et al*. 2008,, 2009). Such data streams might be available and routinely analysed at many other volcanoes elsewhere in soon future.

For the first time, the analysis of optical data allows spatio-temporal investigation of dome growth and collapse. The extruding 2004–2008 Mt. St. Helens spines generally have been described in the literature as being mechanically and/or dynamically solid (Sherrod *et al.* 2008 and references therein). Also DIC strain analysis suggest that the internal structure of the spine is not changing (see Figs 3b and c).

New piece of information is added to the recognition that the spine growth rates have been near steady or even linear in the long term (Dzurisin *et al.* 2008; Major *et al.* 2008, 2009), with minor evidence for a stick slip motion and/or association with earthquakes (Iverson 2008). The difficulty here might be the different sampling frequency of geodetic and seismic data. The incremental vector analysis presented in this work shows that spine growth is highly non-linear (Fig. 4). In general, this finding is not contradicting to the earlier works, but rather highlighting that the long-term steady spine growth may profoundly differ from the short term non-steady spine growth rates. Spine extrusion decelerates before part of the spine collapses and is being integrated into the talus apron. Associated with this mass redistribution, the spine extrusion suddenly increases again. Also the direction of spine extrusion changes to an orientation of $\sim 71^{\circ}$, thus has rotated by almost 20° with respect to the observations prior to the small collapse. An interesting side observation is that also the slump area affecting the upper part of the apron is increasing in velocity and changing direction, implying a direct coupling between dome extrusion and slumping.

The finding of a decreasing extrusion rate prior to a dome sector collapse, followed by acceleration and direction change thereafter,

may lead to further studies regarding the physical processes responsible for the observation. Seismic analysis strongly favoured the dynamics of a stick-slip process, leading to periodic occurrence of earthquakes along the margins of the plug, which itself was forced upwards by ascending, solidifying gas-poor magma (Iverson 2008). Based Newton's second law of motion, one may describe the system in a simplified way, $m(\mathrm{d}u/\mathrm{d}t) + u(\mathrm{d}m/\mathrm{d}t) = pA - mg - F$, where the plug mass is m, the vertical plug velocity is u, gravitational acceleration is g, and the magma pressure against the base of the plug is p, which has an horizontal area A. The right side of the formula describes the magma flow, plug weight and friction force, respectively. Thus a sudden mass change of the plug, for example, if being negative due to sudden collapse, leads to an increase in u.

The deceleration of the spine extrusion, which almost completely stalls immediately prior to the collapse, remains to be analysed, as well as the full duration of the increase in extrusion rate was not further investigated in this work. Given the information available, one may speculate that the extrusion rate reduced due to a combined frictional increase and/or a reduced magma pressure p, which is released by the unloading process. In this view, the sequence of events appear physically closely linked.

Of interest is also, if the finding presented herein for a small scale system is similarly applicable or even observable at larger extrusion domes. This understanding is important as clear correlations exist between dome collapse events and extrusion rates elsewhere, as manifested by major episodes of explosive activity occurring almost immediately after major dome collapse on Soufrière Hills volcano, Montserrat (Druitt *et al.* 2002).

Future studies now have to show the possibility of cross correlating and validating camera strain analysis data with other data sources. Camera monitoring is non-intrusive, which means that no direct access to the near field is required, but it relies on good visibility, which is one of the main shortcomings in respect to other active microwave systems. Optical distortion errors were not corrected in this study, but may introduce spatial errors. Promising for forthcoming studies is to perform a georeferenced strain analysis, which allows cross referencing with supplementary information such as geologic maps.

5. CONCLUSION

Cameras are a becoming an important extension of existing volcano monitoring systems and provide through digital image cross correlation techniques a powerful tool for assessing deformation and strain at centimetre scale. The technique was applied to a sequence of images taken from the spine 7 of the Mount St. Helens dome growth in 2006. Strain analysis suggests the spine to have extruded as a rigid block. A collapse of the block then was associated with a profound change in dome extrusion rate, direction of dome extrusion and associated slumping processes.

ACKNOWLEDGMENTS

The concept and work benefited from numerous discussions I had, especially with M. Shirzaei, E. Holohan, H. Sudhaus, M. Poland and M. Roseneau. Critical and constructive suggestions by two anonymous reviewers are appreciated. Although the data analysis is low cost and easily applicable, the work would not have been possible without the exemplary distribution of time lapse images by staff and scientist of the U.S.G.S. and the David A. Johnston Cascades Volcano Observatory, and the financial support by the GFZ Potsdam.

REFERENCES

Adrian, R.J., 1991. Particle-imaging techniques for experimental fluid mechanics, *Ann. Rev. Fluid Mech.,* **23,** 261–304.

Berthier, E., Vadon, H., Baratoux, D., Arnaud, Y., Vincent, C., Feigl, K.L., Remy, F. & Legresy, B., 2005. Surface motion of mountain glaciers derived from satellite optical imagery, *Remote Sens. Environ.,* **95,** 14–28.

Chivers, K.F. & Clocksin, W.F., 2000. Inspection of surface strain in materials using optical flow, in *Proceedings of the Eleventh British Machine Vision Conference,* Bristol, pp. 392–401.

Clocksin, W.F., Quinta da Fonseca, J., Withers, P.J. & Torr, P.H.S., 2002. Image processing issues in digital strain mapping, *Proc SPIE,* **4790,** 384–395.

Delacourt, C., Allemand, P., Casson, B. & Vadon, H., 2004. Velocity field of the "La Clapière" landslide measured by the correlation of aerial and QuickBird images, *Geophys. Res. Lett.,* **31,** L15619, doi:10.1029/2004GL020193.

Druitt, T.H., *et al*. 2002. Episodes of cyclic vulcanian explosive activity with fountain collapse at Soufriere Hills Volcano, Montserrat, *Mem. Geol. Soc. Lond.,* **21,** 281–306

Dzurisin, D., 2007. *Volcano Deformation; Geodetic Monitoring Techniques,* Praxis Publishing, Chichester, 441pp.

Dzurisin, D., Lisowski, M., Poland, M.P., Sherrod, D.R. & LaHusen, R.G., 2008. Constraints and conundrums resulting from ground-deformation measurements made during the 2004–2005 dome-building eruption of Mount St. Helens, Washington, in *A Volcano Rekindled: The Renewed Eruption of Mount St. Helens, 2004–2006,* US Geol. Surv. Professional Paper 1750, pp. 281–300, eds Sherrod, D.R., Scott, W.E. & Stauffer, P.H., US Geological Survey, Reston, VA.

Gerlach, T.M., McGee, K.A. & Doukas, M.P., 2008. Emission rates of CO_2, SO_2, and H_2S, scrubbing, and preeruption excess volatiles at Mount St. Helens, 2004–2005, in *A Volcano Rekindled: The Renewed Eruption of Mount St. Helens, 2004–2006,* US Geol. Surv. Professional Paper 1750, pp. 543–572, eds Sherrod, D.R., Scott, W.E. & Stauffer, P.H., US Geological Survey, Reston, VA.

Hauser, C. & Walz, B., 2004. Bildbasierte Verformungsmessung mit der PIV-Methode. Image-based deformation measurement using the PIV method, *Geotechnik,* **27** (4), 339–343.

Horn, B.K.P. & Schunck, B.G., 1981. Determining optical flow, *Artif. Intell.,* **17,** 185–203.

Iverson, R.M., 2008. Dynamics of seismogenic volcanic extrusion resisted by a solid surface plug, Mount St. Helens 2004–2005, in *A Volcano Rekindled: The Renewed Eruption of Mount St. Helens, 2004–2006,* US Geol. Surv. Professional Paper 1750, pp. 425–460, eds Sherrod, D.R., Scott, W.E. & Stauffer, P.H., US Geological Survey, Reston, VA.

Johnson, J.B., Lees, J.M., Gerst, A., Sahagian, D. & Varley, N., 2008. Long-period earthquakes and co-eruptive dome inflation seen with particle image velocimetry, *Nature,* **456**(7220), 377–381.

Kaab, A., 2002. Monitoring high-mountain terrain deformation from repeated air- and spaceborne optical data: examples using digital aerial imagery and ASTER data, *ISPRS J. Photogr. Remote Sens.,* **57,** 39–52.

Major, J.J., Dzurisin, D., Schilling, S.P. & Poland, M.P., 2009. Monitoring lava-dome growth during the 2004–2008 Mount St. Helens, Washington, eruption using oblique terrestrial photography, *Earth planet. Sci. Lett.,* **286** (1–2), 243–254.

Major, J.J., Kingsbury, C.G., Poland, M.P. & LaHusen, R.G., 2008. Extrusion rate of the Mount St. Helens lava dome estimated from terrestrial imagery, November 2004–December 2005, in *A Volcano Rekindled: The Renewed Eruption of Mount St. Helens, 2004–2006,* US Geol. Surv. Professional Paper 1750, pp. 237–256, eds Sherrod, D.R., Scott, W.E. & Stauffer, P.H., US Geological Survey, Reston, VA.

Pallister, J.S., Thornber, C.R., Cashman, K.V., Clynne, M.A., Lowers, H.A., Mandeville, C.W., Brownfield, I.K. & Meeker, G.P., 2008. Petrology of the 2004–2006 Mount St. Helens lava dome—implications for magmatic plumbing and eruption triggering, in *A Volcano Rekindled: The Renewed*

Eruption of Mount St. Helens, 2004–2006, US Geol. Surv. Professional Paper 1750, pp. 647–702, eds Sherrod, D.R., Scott, W.E. & Stauffer, P.H., US Geological Survey, Reston, VA.

Pan, B., Qian, K., Xie, H. & Asundi, A., 2009. Two-dimensional digital image correlation for in-plane displacement and strain measurement: a review, *Meas. Sci. Technol.,* **20,** 062001, doi:10.1088/0957-0233/20/6/062001.

Poland, M.P. *et al.*, 2008. Remote camera observations of lava dome growth at Mount St. Helens, Washington, October 2004 to February 2006, in *A Volcano Rekindled: The Renewed Eruption of Mount St. Helens, 2004–2006,* US Geol. Surv. Professional Paper 1750, pp. 225–236, eds Sherrod, D.R., Scott, W.E. & Stauffer, P.H., US Geological Survey, Reston, VA.

Quinta da Fonseca, J., Mummery, P.M. & Withers, P.J., 2005. Full-field strain mapping by optical correlation of micrographs acquired during deformation, *J. Microsc.,* **218,** 9–21.

Scambos, T.A., Dutkiewicz, M.J., Wilson, J.C. & Bindschadler, R.A., 1992. Application of image cross-correlation to the measurement of glacier velocity using satellite image data, *Remote Sens. Environ.,* **42,** 177–186.

Schreier, H.W., Braasch, J.R. & Sutton, M.A., 2000. On systematic errors in digital image correlation, *Opt. Eng.,* **39** (11), 2915–2921.

Sherrod, D.R., Scott, W.E. & Stauffer, P.H., 2008. A volcano rekindled; the renewed eruption of Mount St. Helens, 2004–2006, pp. 856.

Vallance, J.W., Schneider, D.J. & Schilling, S.P., 2008. Growth of the 2004–2006 lava-dome complex at Mount St. Helens, Washington, in *A Volcano Rekindled: The Renewed Eruption of Mount St. Helens, 2004–2006,* US Geol. Surv. Professional Paper 1750, pp. 169–208, eds Sherrod, D.R., Scott, W.E. & Stauffer, P.H., US Geological Survey, Reston, VA.

Van Puymbroeck, N., Michel, R., Binet, R., Avouac, J.P. & Taboury, J., 2000, Measuring earthquakes from optical satellite images, *Appl. Opt. Inform. Process.,* **39,** 1–14.